Structural Basis for Putrescine Activation of Human *S*-Adenosylmethionine Decarboxylase[†,‡]

Shridhar Bale,[§] Maria M. Lopez,[||,#] George I. Makhatadze,[||,#] Qingming Fang,[⊥] Anthony E. Pegg,[⊥] and Steven E. Ealick*[,§]

Department of Chemistry and Chemical Biology, Cornell University, Ithaca, New York 14853, Department of Biochemistry and Molecular Biology, Milton S. Hershey Medical Center, Pennsylvania State University College of Medicine, Hershey, Pennsylvania 17033, and Departments of Cellular and Molecular Physiology and Pharmacology, Milton S. Hershey Medical Center, Pennsylvania State University College of Medicine, Hershey, Pennsylvania 17033

Received September 10, 2008; Revised Manuscript Received October 2, 2008

ABSTRACT: Putrescine (1,4-diaminobutane) activates the autoprocessing and decarboxylation reactions of human *S*-adenosylmethionine decarboxylase (AdoMetDC), a critical enzyme in the polyamine biosynthetic pathway. In human AdoMetDC, putrescine binds in a buried pocket containing acidic residues Asp174, Glu178, and Glu256. The pocket is away from the active site but near the dimer interface; however, a series of hydrophilic residues connect the putrescine binding site and the active site. Mutation of these acidic residues modulates the effects of putrescine. D174N, E178Q, and E256Q mutants were expressed and dialyzed to remove putrescine and studied biochemically using X-ray crystallography, UV-CD spectroscopy, analytical ultracentrifugation, and ITC binding studies. The results show that the binding of putrescine to the wild type dimeric protein is cooperative. The D174N mutant does not bind putrescine, and the E178Q and E256Q mutants bind putrescine weakly with no cooperativity. The crystal structure of the mutants with and without putrescine and their complexes with *S*-adenosylmethionine methyl ester were obtained. Binding of putrescine results in a reorganization of four aromatic residues (Phe285, Phe315, Tyr318, and Phe320) and a conformational change in the loop 312−320. The loop shields putrescine from the external solvent, enhancing its electrostatic and hydrogen bonding effects. The E256Q mutant with putrescine added shows an alternate conformation of His243, Glu11, Lys80, and Ser229, the residues that link the active site and the putrescine binding site, suggesting that putrescine activates the enzyme through electrostatic effects and acts as a switch to correctly orient key catalytic residues.

S-Adenosylmethionine decarboxylase (AdoMetDC[1]) is a critical enzyme in the polyamine biosynthetic pathway (*1, 2*) and depends on a pyruvoyl group for the decarboxylation reaction (*3*−*5*). It is synthesized as a proenzyme that undergoes an apparent autocatalytic processing reaction to generate the pyruvoyl group from an internal serine residue. The enzyme converts *S*-adenosylmethionine (AdoMet) to *S*-adenosyl-5′-(3-methylthiopropylamine) (dcAdoMet). The propylamine group from the product is transferred to putrescine to form spermidine or spermidine to form spermine. Putrescine is generated by the decarboxylation of ornithine by ornithine decarboxylase (ODC). Polyamine levels are highly regulated in the cell and are closely linked to normal cell growth and division. Both ODC and AdoMetDC are regulated through multiple mechanisms, catalyze reactions in the earlier stages of polyamine biosynthesis, and their reaction products are committed to polyamine biosynthesis. Consequently, these enzymes are the focus of inhibitor design, for both anticancer and antiparasitic agents (*6, 7*). α-Difluoromethylornithine is a suicide inhibitor of ODC and is approved by the Food and Drug Administration for the treatment of African sleeping sickness. Two inhibitors of AdoMetDC, methylglyoxal *bis*(guanylhydrazone) and 4-amidinoindan-1-one-2′-amidinohydrazone (CGP48664A), have been the subject of several clinical trials (*8*−*16*). Although neither compound is approved for clinical use, the polyamine biosynthetic pathway remains an attractive target for both cancer and antiparasitic chemotherapy.

[†] This work was supported by the Biomedical Research Resource Program (RR-01646 and RR-15301) and the National Cancer Institute (Grant CA-094000 to SEE and Grant CA-18138 to A.E.P.) of the National Institutes of Health. S.E.E. is also indebted to the W. M. Keck Foundation and the Lucille P. Markey Charitable Trust.

[‡] The Protein Data Bank codes for the mutants and complexes are under the following accession numbers: AdoMetDC(−Put), 3EP9; D174N(−Put), 3EP3; E256Q(−Put), 3EP4; E178Q(−Put), 3EP5; D174N(−Put)/MeAdoMet, 3EP6; E256Q(−Put)/MeAdoMet, 3EP7; E178Q(−Put)/MeAdoMet, 3EP8; E178Q(+Put), 3EPA; E256Q(+Put), 3EPB.

* To whom correspondence should be addressed. Tel: (607) 255-7961. Fax: (607) 255-1227. E-mail: see3@cornell.edu.

[§] Cornell University.

[||] Department of Biochemistry and Molecular Biology, Pennsylvania State University College of Medicine.

[⊥] Departments of Cellular and Molecular Physiology and Pharmacology, Pennsylvania State University College of Medicine.

[#] Present address: Center for Biotechnology and Interdisciplinary Studies, Rensselaer Polytechnic Institute, 110 Eighth Street, Troy, NY 12180.

[1] Abbreviations: AdoMetDC, *S*-adenosylmethionine decarboxylase; MeAdoMet, *S*-adenosylmethionine methyl ester; Put, putrescine; AdoMet, *S*-adenosylmethionine; dcAdoMet, *S*-adenosyl-5′-(3-methylthiopropylamine); ODC, ornithine decarboxylase; ITC, isothermal titration calorimetry; DTT, dithiothreitol; WT, wild type; TCEP, tris(2-carboxyethyl)phosphine; EDTA, ethylenediaminetetraacetic acid.

10.1021/bi801732m CCC: $40.75
Published on Web 11/17/2008

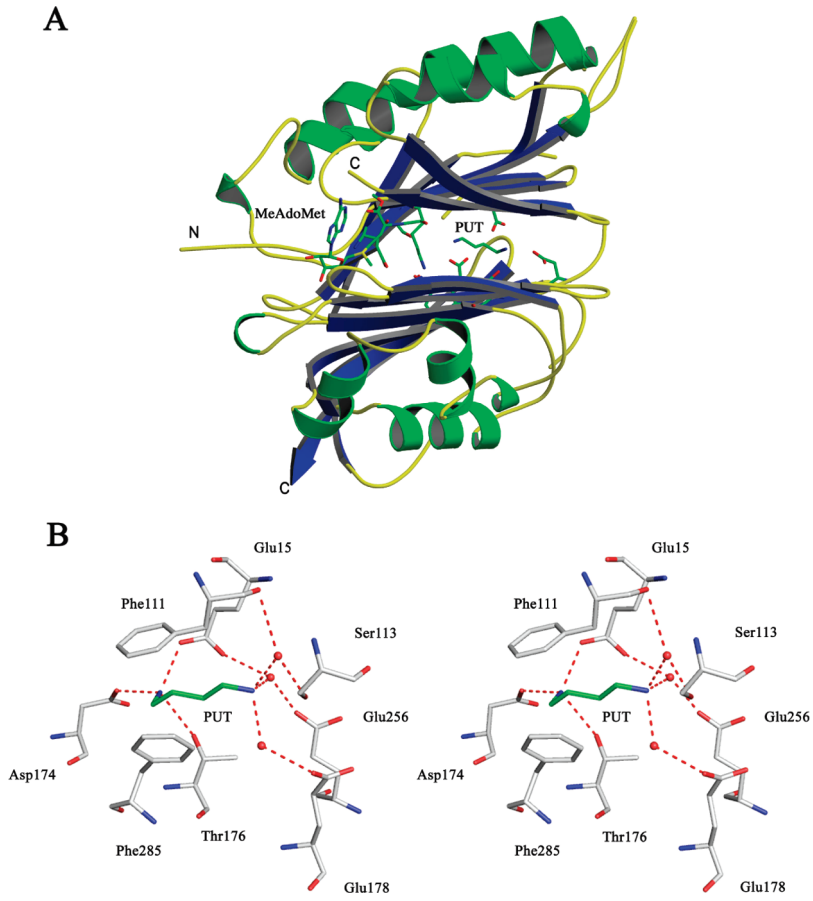

FIGURE 1: Putrescine binding site of human AdoMetDC. (A) Ribbon diagram of AdoMetDC showing the putrescine binding site and the active site with MeAdoMet bound (from pdb 1I7B). (B) Stereoview of interactions of putrescine with the enzyme. Putrescine carbon atoms are colored green. Water molecules are shown as red spheres, and hydrogen bonds are shown as dashed lines.

All AdoMetDCs currently characterized are pyruvoyl enzymes, but they can be divided into two classes. Class 1 enzymes are present in bacteria and archaea, and class 2 enzymes are present in eukaryotes (*5, 17*). The human AdoMetDC proenzyme contains 334 amino acid residues. The processing reaction generates the α- (67 amino acids) and β-subunits (266 amino acids) with the pyruvoyl group at the N-terminus of the β-subunit (*18*). Only a small fraction of the total AdoMet pool is in the decarboxylated form, and AdoMetDC activity is very highly regulated according to the need for polyamine synthesis (*3, 19, 20*). An important part of this regulation in mammalian cells and some other eukaryotes with class 2 AdoMetDCs, but not in plants, is the activation of the enzyme by putrescine (*3, 19*−*21*). Activation of the mammalian enzyme occurs at two stages: the rate of processing of the proenzyme is stimulated, and the decarboxylase activity is increased in the presence of putrescine (*22, 23*). These factors provide a link between the availability of putrescine and the production of dcAdoMet, which is the other substrate of spermidine synthase. This allows the very efficient conversion of putrescine into spermidine without increasing the steady state pool of dcAdoMet. Mammalian cells therefore have spermidine content greatly in excess of putrescine, and c.1−2% of the AdoMet is in the form of dcAdoMet (*20, 24, 25*). AdoMetDCs from fungi and several protozoal parasites have also been shown to be activated by putrescine (*20, 22, 26, 27*), but this activation may occur only at the level of the stimulation of activity (*28, 29*).

Structural studies of human AdoMetDC have indicated that the functional form of human AdoMetDC is an $(\alpha\beta)_2$ dimer with one active site and one pyruvoyl cofactor per protomer (*23, 30, 31*). The putrescine binding site is located between two central β-sheets of the enzyme, away from the active site and near the dimer interface (Figure 1A). One end of putrescine is directly hydrogen bonded to Asp174, Glu15, and Thr176. The other end is hydrogen bonded through water molecules to Glu178, Glu15, Glu256, and Ser113. The aliphatic chain of putrescine stacks against Phe285 and Phe111 (Figure 1B). The putrescine molecule is linked to the active site by several buried charged residues. Mutations of residues in the putrescine binding site modulate the effects of putrescine (*32*). Studies using site-directed mutagenesis of the human and *T. cruzi* AdoMetDCs have identified multiple residues whose alteration abolished the activation (*22, 29, 32*−*34*). These include Asp174 in the human enzyme, which is conserved in all of the known putrescine-stimulated AdoMetDCs and is not present in other class 2 AdoMetDCs such as those from plants, which are not putrescine activated (*33, 35*).

MATERIALS AND METHODS

Apart from these studies, there is virtually no information on the binding of putrescine to human AdoMetDC or the changes brought about by this binding. To obtain further insights into the mechanism of putrescine activation, we undertook structural studies of human AdoMetDC and putrescine binding mutants D174N, E178Q, and E256Q, with

(+Put) and without (−Put) bound putrescine. We have also studied the biochemical properties of the putrescine free enzymes using UV-CD spectroscopy, analytical ultracentrifugation, and isothermal titration calorimetry (ITC). The crystal structures showed no global structural changes but revealed a local rearrangement of four aromatic residues near the putrescine binding site, Phe285, Phe315, Tyr318, and Phe320, and a conformational change in the loop 312−320. Biophysical studies confirmed one putrescine binding site per protomer and showed positive cooperativity between the two binding sites within the dimer. Additionally, the D174N mutant did not bind putrescine, and the E178Q and E256Q mutants bind putrescine weakly with no cooperativity. Our findings demonstrate that putrescine activates AdoMetDC primarily through positioning of active site residues and electrostatic effects relayed to the active site largely through hydrogen bonding.

Cloning and Expression. The constructs for expression of human AdoMetDC and mutants were modified from those described previously (*18, 32*−*34*) to place the $(His)_6$ tag at the carboxyl end of the protein replacing the C-terminal -QQQQQS sequence. Briefly, primers 5′-d(ATTAAAGAG-GAGAAATTAACTATGGAAGCTGCACATTT-TTTC)-3′ with a Bser I site (underlined) and 5′-(GTGGTGGGAT-TCACTCTGCTGTTG-TTGCTG)-3′ with a BamH I site (underlined) were used as the sense and antisense primers in a PCR reaction using pQE-SAMDC as a template. The product was digested with Bser I and BamH1 and ligated into plasmid pQE-C145S (*36*), which encodes the C-terminal $(His)_6$-tag, that had been digested with the same enzymes. *E. coli* strain BL21(DE3) containing the AdoMetDC wild type plasmid or plasmid for the mutant proteins was grown at 30 °C overnight in a 2× YT media containing 100 μg/mL ampicillin. The protein expression was induced by addition of 1 mM isopropyl-1-thio-β-D-galactopyranoside. Cells were harvested after 4 h and resuspended in 50 mM sodium phosphate at pH 8.0, 200 mM NaCl, 2.5 mM putrescine, and 0.1 mM phenylmethylsulfonyl fluoride. The cells were lysed using a French pressure cell. The wild type AdoMetDC and mutants were purified using a Ni-NTA (Qiagen) affinity column under native conditions in the presence of 2.5 mM putrescine. Fractions containing the desired protein were combined and concentrated by ammonium sulfate precipitation (80%). The pellet was dissolved and dialyzed against 50 mM phosphate, 200 mM NaCl, 1 mM ethylenediaminetetraacetic acid (EDTA), and 1 mM tris(2-carboxyethyl)phosphine (TCEP) and loaded onto a Sephacryl S-200 HR equilibrated in the same buffer and connected to an AKTA (Pharmacia) chromatography system. The eluted pure protein was concentrated by ammonium sulfate precipitation (80%), dissolved, and dialyzed against 50 mM sodium phosphate pH 7.5, 1 mM TCEP, and 1 mM EDTA. The concentrated protein was kept at −80 °C. The purified protein correctly processed into a 31 kDa α subunit and a 7.5 kDa β subunit as judged by SDS−PAGE electrophoresis. The protein concentration was calculated spectrophotometrically using the extinction coefficient ε_{280} = 39,400 M^{-1} cm^{-1}. Corrections for light scattering were taken into account (*37*).

CD Spectroscopy. The CD experiments were performed using a Jasco J-715 automatic recording spectrapolarimeter. Spectra were recorded at 20 °C in10 mM phosphate at pH 7.5, 0.2 mM EDTA, and 0.2 mM TCEP in the absence and presence of putrescine. Near-UV CD spectra were recorded in a 1 cm rectangular quartz cell. The protein concentration was 15 μM. The Far-UV CD spectra were recorded in a 1 mm cylindrical quartz cell. The protein concentration was 2.5 μM. The putrescine concentration was 4-fold higher than the wild type or 40-fold higher than the variant proteins to ensure that the proteins were saturated with putrescine. The molar ellipticity, [Θ], was calculated as:

$$[\Theta] = \frac{\Delta\Theta \cdot Mw}{10 \cdot l \cdot c} \quad (1)$$

where *Mw* is the mean molecular mass of amino acid residues in AdoMetDC (115 Da), *c* is the protein concentration in mg/mL, and *l* is the optical path length in centimeters.

Analytical Ultracentrifugation. Equilibrium sedimentation experiments were performed using a Beckman XL-A analytical ultracentrifuge with an AN-60Ti rotor, operating at 4 °C. Samples were loaded into two-sector cells and spun at three different speeds (12,000, 15,000, and 20,000 rpm). The absorbance at 280 nm, *A*, was recorded as a function of the radial position, *r*. Equilibrium was considered to be attained when replicate scans separated by 6 h were indistinguishable. The data sets for each protein were globally fitted according to a model in which single species are present in solution:

$$A = I + A_o \cdot \exp \frac{(M \cdot (r^2 - r_o^2))}{\left(\frac{2 \cdot R \cdot T}{(1 - \rho \cdot \nu) \cdot \omega^2}\right)} \quad (2)$$

where *I* is the baseline offset constant, *M* is the molecular weight of the species present in solution, ν is the partial specific volume (0.749 cm^3/g) calculated as described in ref *38*, ω is the angular velocity, *R* is the gas constant in erg/(mol·K), *T* is the temperature in Kelvin, and ρ is the density of the solvent (1 g/cm^3). The goodness of the fit was assessed by the quality of the residuals.

Isothermal Titration Calorimetry. The ITC experiments were performed using a VP-ITC titration microcalorimeter (MicroCal, Inc.). The procedure for these experiments has been described previously (*39*). In brief, the experiments were performed by injecting 3−10 μL of putrescine with concentrations ranging between 0.7 and 16 mM into the sample cell containing the protein solution. The protein concentration varied between 12 and 87 μM, depending on the magnitude of the heat effects observed. The buffer used was 50 mM phosphate at pH 7.5, 1 mM EDTA, and 1 mM TCEP. Dilution effects were taken into account by injecting the putrescine solution into the buffer. The heat of the reaction after each injection, q_i, was obtained by integrating the peak after the injection using the ORIGIN software provided by the manufacturer. The binding isotherms were fitted to a single set of sites (as described previously (*40*)), model 1 in which 2 molecules of putrescine bind to the dimeric protein according to Scheme 1.

The heat of the reaction, *Q*, is defined as follows:

$$Q = \Delta H \cdot \frac{A - \sqrt{A^2 - 4 \cdot n \cdot [L]_T \cdot [M]_T}}{2 \cdot [M]_T}$$
$$\text{where } A = [M]_T + n \cdot [L]_T + (1/K) \quad (3)$$

Scheme 1

$$M_2 + 2 \cdot L \xleftrightarrow{K} M_2L_2$$

Scheme 2

$$M_2 + L \xleftrightarrow{K_1} M_2L \xleftrightarrow{K_2} M_2L_2$$

where $[M]_T$ is the total protein concentration expressed per monomer, $[L]_T$ is the total putrescine concentration, n is the stoichiometry of the interaction, ΔH is the enthalpy of binding, and K is the equilibrium constant.

Putrescine binding to wild type AdoMetDC was also fitted according to model 2 (Scheme 2) (*41*).

The heat of the reaction expressed per mol of protein relates to the thermodynamic parameters as follows:

$$Q = \frac{K_1 \cdot [L] \cdot \Delta H_1 + K_1K_2 \cdot [L]^2 \cdot (\Delta H_1 + \Delta H_2)}{(1 + K_1 \cdot [L] + K_1 \cdot K_2 \cdot [L]^2)} \quad (4)$$

ΔH_1 and ΔH_2 are the enthalpies of binding the first and second putrescine molecule, respectively. ΔH_1 and ΔH_2 are both expressed per mol of monomer. K_1 and K_2 are the apparent binding constants under the approximation that the free putrescine concentration is equal to the total concentration.

The populations of each species in equilibrium were calculated as follows:

$$\frac{[M_2]}{[M_T]} = \frac{1}{(1 + K_1 \cdot [L] + K_1 \cdot K_2 \cdot [L]^2)} \quad (5)$$

$$\frac{[M_2L]}{[M_T]} = \frac{K_1 \cdot [L]}{(1 + K_1 \cdot [L] + K_1 \cdot K_2 \cdot [L]^2)} \quad (6)$$

$$\frac{[M_2L_2]}{[M_T]} = \frac{K_1 \cdot K_2 \cdot [L]^2}{(1 + K_1 \cdot [L] + K_1 \cdot K_2 \cdot [L]^2)} \quad (7)$$

Fits to eqs 3 and 4 were done using nonlinear fitting routine NLREG (http://www.nlreg.com/), as described previously (*42*).

Putrescine Analysis. Putrescine was released from bound protein by treatment with perchloric acid and determined by reverse-phase HPLC using postcolumn derivatization with *o*-phthalaldehyde and fluorescence detection (*43*).

Crystallization Conditions. The protein was buffer exchanged into 10 mM *N*-(2-hydroxyethyl)piperazine-*N*′-2-ethanesulfonic acid, pH 7.5, 200 mM NaCl, and 1 mM dithiothreitol (DTT) using Bio-Rad buffer exchange chromatography columns. For crystallization, the concentration of the protein was maintained at 10 mg/mL for the E178Q(−Put) mutant and at 5 mg/mL for the D174N(−Put) and E256Q(−Put) mutants. The crystals were grown using the hanging drop method at 22 °C in 13−16% polyethylene glycol 8000, 100 mM tris(hydroxymethyl)aminomethane, pH 7.5−8.5, and 10 mM DTT. The crystals grew to a maximum size of 0.2 mm × 0.15 mm × 0.1 mm in 2−3 days. For the complexes of the mutants with MeAdoMet, each of the mutants was incubated with 4−6 molar excess of MeAdoMet for 24 h prior to crystallization. To obtain structures of the mutants with putrescine bound, the E178Q and E256Q mutant proteins were incubated with 4−6 molar excess of putrescine for 2 h prior to crystallization.

Data Collection and Processing. The data for the D174N(−Put), E178Q(−Put), and E256Q(−Put) were collected at the A1 station of the Cornell High Energy Synchrotron Source (CHESS) using a ADSC Quantum 210 detector. Data for D174N(−Put) and E256Q(−Put) were collected over 180° with a 1° oscillation angle and 30 s exposure time per image at a crystal to detector distance of 175 mm. Data for the E178Q(−Put) were collected over 110° with a 1° oscillation angle and 60 s exposure time per image at a crystal to detector distance of 185 mm. The data for the putrescine free mutant complexes with MeAdoMet and E178Q(+Put) and E256Q(+Put) were collected at NE-CAT beamlines 24-ID-C and 24-ID-E, respectively, at the Advanced Photon Source (APS). Data were collected over a range of 160°−360° with a 1 s exposure time and a 1° oscillation range. The crystal to detector distance varied between 200−280 mm. The data for the wild type AdoMetDC-(−Put) were collected at a home source using a Rigaku R-Axis^{++} detector and Cu Kα radiation from a Rigaku RU-300 rotating anode generator. Data were collected over 140° with a 0.5° oscillation angle and 20 min exposure per oscillation with a crystal to detector distance of 180 mm. The crystals were sequentially transferred to solutions with 2%, 5%, 8%, 15%, and 18% glycerol with 1−2 min equilibration between each step. The crystals were flash frozen under liquid nitrogen for the MeAdoMet complexes and putrescine bound mutants and the crystals were directly flash frozen under a liquid nitrogen stream for putrescine free mutants and AdoMetDC(−Put). The data were indexed, integrated, and scaled using the HKL2000 program suite (*44*). The data collection statistics are summarized in Table 1.

Structure Determination and Refinement. All of the structures were determined by molecular replacement using CNS (*45*). The structure of AdoMetDC(+Put)/MeAdoMet (PDB ID 1I7B), minus pyruvoyl group, putrescine, MeAdoMet, and water molecules, was used as the search model. The model building for the E178Q(−Put) structure was done using the program O (*46*). The model building for the rest of the structures was done using the program COOT (*47*). The refinement process included successive rounds of simulated annealing, minimization, B-factor refinement, calculation of composite omit maps, difference Fourier maps, and model building. After a few rounds of refinement, the improved difference $F_o - F_c$ Fourier map was used to identify ligands. The ligand was then added to the model followed by another round of refinement and picking of water molecules. The parameter and the topology files for MeAdoMet were generated using the HIC-Up server (*48*). The difference $F_o - F_c$ Fourier map was also used to identify conformational changes of residues in the putrescine binding site as well as the active site. The final refinement statistics are given in Table 2. A difference distance matrix program was used to identify conformational changes in the backbone of the protein structure (*49, 50*).

RESULTS

Studies were carried out with wild type AdoMetDC and three mutants of the protein in which acidic residues that hydrogen bond with putrescine (Figure 1B) were altered to the corresponding amides. The proteins were dialyzed extensively to remove bound putrescine. Direct analysis of

Table 1: Data Collection Statistics for AdoMetDC Mutants and Complexes[a]

	D174N (−Put)	E256Q (−Put)	E178Q (−Put)	D174N (−Put)/ MeAdoMet	E256Q (−Put)/ MeAdoMet	E178Q (−Put)/ MeAdoMet	AdoMetDC (−Put)	E178Q (+Put)	E256Q (+Put)
wavelength	0.9764	0.9764	0.9766	0.9795	0.9795	0.9795	1.5418	0.9792	0.9792
space group (Å)	C2	C2	C2	C2	C2	C2	C2	C2	C2
a (Å)	90.60	90.71	90.57	99.22	94.44	100.15	90.57	91.60	92.35
b (Å)	55.24	55.90	56.26	50.60	50.08	51.07	55.54	54.49	53.54
c (Å)	74.22	74.33	74.05	68.82	70.17	68.95	74.31	74.58	74.71
β (°)	109.64	109.84	109.73	104.95	105.00	105.40	109.66	109.45	109.09
resolution (Å)	1.84	1.88	1.98	1.70	2.00	1.97	2.35	2.10	1.75
total reflections	88255	71106	53478	122776	54248	73956	41261	69216	123289
unique reflections	27642	27282	21433	35113	18180	23589	14524	19713	34072
redundancy	3.2(2.8)	2.6(2.3)	2.5(2.2)	3.5(2.5)	2.9(2.7)	3.1(2.5)	2.8(2.6)	3.5(2.8)	3.6(3.0)
% completeness	92.1(73.8)	96.7(87.0)	89.8(89.4)	96.3(78.0)	84.0(72.6)	98.6(91.1)	99.1(95.7)	96.8(79.8)	97.7(89.6)
I/σ	15.9(2.2)	16.0(2.0)	14.4(2.0)	15.4(2.2)	9.9(3.3)	15.0(3.4)	13.9(2.0)	34.4(6.2)	30.1(4.6)
*R*sym[b]	6.4(39.0)	4.9(39.6)	7.1(43.8)	8.3(32.8)	10.7(25.6)	8.0(23.8)	9.1(46.8)	3.7(12.2)	4.2(15.8)
Matthew's coef. (Å^3/Da)	2.28	2.31	2.32	2.18	2.09	2.22	2.30	2.29	2.28
solvent content (%)	45.1	45.9	45.9	42.5	40.1	43.5	45.5	45.3	45.0

[a] The values in parenthesis are for the highest resolution shell. [b] $R_{sym>}=\Sigma\Sigma_i|I_i - \langle I\rangle|/\Sigma\langle I\rangle$, where $\langle I\rangle$ is the mean intensity of the N reflections with intensities I_i and common indices h,k,l.

Table 2: Refinement Statistics for AdoMetDC Mutants and Complexes

	D174N (−Put)	E256Q (−Put)	E178Q (−Put)	D174N (−Put)/ MeAdoMet	E256Q (−Put)/ MeAdoMet	E178Q (−Put)/ MeAdoMet	AdoMetDC (−Put)	E178Q (+Put)	E256Q (+Put)
resolution (Å)	1.84	1.88	1.98	1.70	2.00	1.97	2.35	2.10	1.75
R-factor[a]	0.243	0.229	0.214	0.217	0.226	0.209	0.228	0.222	0.238
R-free[b]	0.282	0.262	0.246	0.240	0.251	0.237	0.274	0.250	0.253
				No of Non-H Atoms					
protein	2411	2413	2411	2415	2412	2413	2443	2498	2500
ligand	8	8	12	28	28	28	8	14	6
water	179	148	103	163	186	206	103	138	194
				B-Factors					
protein (Å^2)	46.4	46.1	37.7	31.0	35.4	29.5	50.1	40.4	31.8
ligand (Å^2)	82.0	64.0	44.4(44.6)	32.8	40.1	44.0	84.9	71.2(39.7)	28.6
				rms Deviations					
bonds (Å)	0.007	0.008	0.006	0.010	0.022	0.014	0.007	0.010	0.016
angles	1.3	1.3	1.3	1.4	1.7	1.6	1.3	1.4	1.5
dihedrals	25.8	25.7	25.5	25.6	25.6	25.4	24.4	25.7	26.4
				Ramachandran Plot					
most favored region (%)	90.0	90.4	93.1	91.6	90.3	91.2	86.6	91.2	89.7
additional favored region (%)	8.9	8.8	6.2	6.9	9.3	7.7	11.9	8.1	10.3
generously allowed region (%)	0.8	0.8	0.8	1.5	0.0	1.2	1.5	0.7	0.0
disallowed region (%)	0.4	0.0	0.0	0.0	0.4	0.0	0.0	0.0	0.0

[a] R-factor $= \Sigma_{hkl}||F_{obs}| - k|F_{cal}||/\Sigma_{hkl}|F_{obs}|$, where F_{obs} and F_{cal} are observed and calculated structure factors, respectively. [b] In R-free, the sum is extended over a subset of reflections (5%) that were excluded from all stages of refinement.

the protein preparations confirmed that they contained <0.001 mol putrescine/mol protein.

Far-UV and Near-UV CD. Far-UV CD spectroscopy was used to assess the effect of substitutions and putrescine binding on the secondary structure of the protein. Figure 2A shows the Far-UV CD spectra for the wild type AdoMetDC mutants. In all cases, the spectra show a minimum at 218 nm and a maximum at 195 nm, typical of proteins with significant β-sheet content. The difference in ellipticity among the proteins is within the experimental error indicating that these single amino acid substitutions did not perturb the secondary structure of AdoMetDC. Figure 2A inset shows the effect of putrescine binding on the wild type AdoMetDC secondary structure. It can be seen that the holo protein has overall the same secondary structure as the apo form. The small difference observed might be due to contributions of the aromatic residues, which interact with putrescine (Phe111, Phe285, Tyr318, Phe315, and Phe320) (*23, 30, 31*).

Near-UV CD is very sensitive to the environment of aromatic side chains and therefore to the tertiary structure of the protein. Figure 2B shows the near-UV CD spectra for the AdoMetDC wild type and variant proteins. The overall shapes of the spectra are similar with a minimum at 278 nm and a maximum at 256 nm. The small difference in absolute values observed among proteins is probably due to the slightly different orientation of the aromatic residues caused by the substitutions. Putrescine has a small effect on the near-UV CD for the wild type and E256Q proteins (Figures 2C and D, respectively). Under saturated conditions of putrescine, the ligand causes a small increase in ellipticity, probably due to a more rigid environment of the aromatic residues. However, no change in ellipticity was observed for

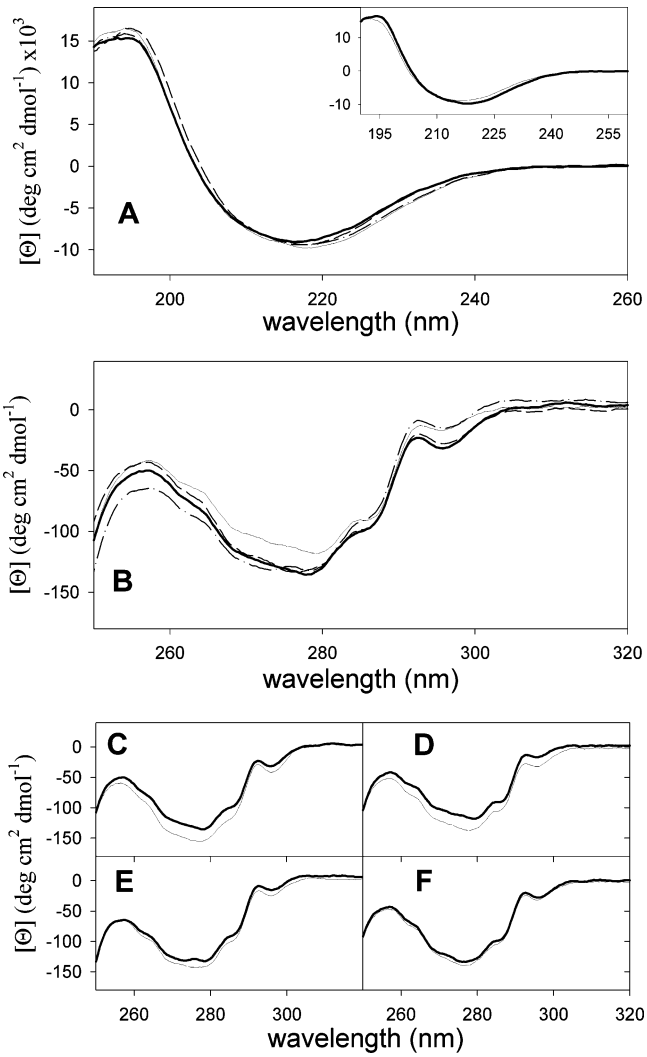

FIGURE 2: (A) Effect of mutations on the Far-UV CD spectra for human wild type AdoMetDC (thick solid line), E256Q (thin solid line), D174N (dashed line), and E178Q (dashed-and-dotted line). Inset: Effect of putrescine on the Far-UV CD spectra; wild type protein in the absence (thick solid line) and presence (thin solid line) of putrescine. (B) Effect of mutations on the Near-UV CD spectra for wild type AdoMetDC (thick solid line), E256Q (thin solid line), D174N (dashed line), and E178Q (dashed-and-dotted line). Effect of putrescine on the Near-UV CD spectra: wild type AdoMetDC(C), E256Q (D), E178Q (E), and D174N (F) in the absence (thick solid line) and presence (thin solid line) of putrescine.

E178Q and D174N, respectively (Figures 2E and F, respectively). This is expected for D174N as the substitution abolishes putrescine binding to the protein (see later Results).

Analytical Ultracentrifugation of the AdoMetDC Proteins. The X-ray structure of the human wild type AdoMetDC shows that the protein crystallizes as a dimer (*18, 23*). To assess if this is the functional unit in solution and if the putrescine or mutations affect the oligomerization state of the protein, sedimentation equilibrium experiments were performed at three different speeds. For each protein, the data were globally fitted according to different oligomeric models. In all cases, the experimental data were best fitted according to the single ideal species model (eq 2 in Materials and Methods) and a molecular weight of a dimer. Figure 3 shows representative data for the wild type AdoMetDC. The molecular weight obtained from the global fit was 77.2 ± 0.3 kDa in very good agreement with the theoretical one (76.8 kDa). These results suggest that the monomers of AdoMetDc interact with high affinity. We estimated the upper limit for the dimerization constant to be in the order of 3×10^7 M^{-1}.

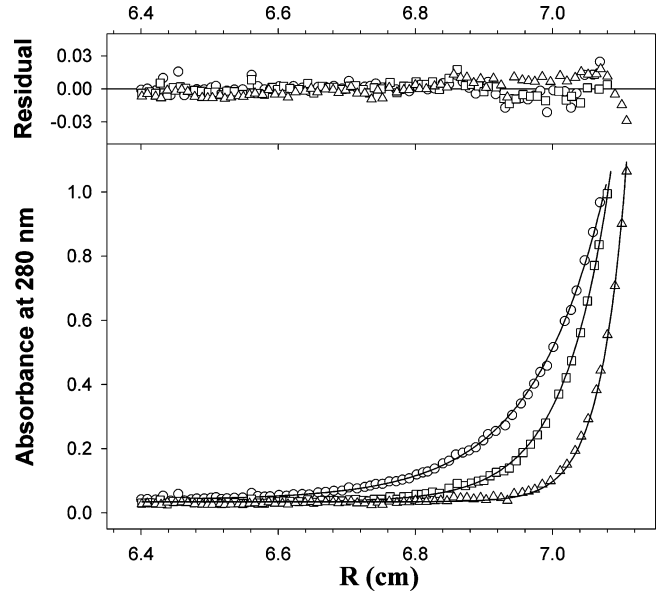

FIGURE 3: Equilibrium sedimentation analysis of human AdoMetDC. Representative traces for the wild type AdoMetDC at 12,000 (circles), 15,000 (squares), and 20,000 rpm (triangles). Solid lines represent the global fit according to eq 2. The molecular weight obtained from the fit was (77.2 ± 0.1) kDa.

Putrescine Binding to AdoMetDC Characterized by ITC. In the ITC experiments, the heat released upon putrescine binding to the proteins was measured. Figure 4A shows representative heat effects for putrescine binding to wild type AdoMetDC at 15 °C. The heat of binding is proportional to the enthalpy and degree of binding and thus allows model dependent estimates of the enthalpy (ΔH), the binding constant (K), and the stoichiometry (n). Figure 4B shows the binding isotherm in which the heat effect is plotted as a function of putrescine concentration. The experimental data were fitted according to eq 3 (in Materials and Methods), which considers independent and noninteractive binding sites (Scheme 1). The n parameter was kept constant as 1 molecule of putrescine per monomer of wild type AdoMetDC. It can be seen that the fit to model 1 does not represent the experimental data. The binding isotherm was then fitted according to eq 4 (in Materials and Methods), which considers two interactive ligand binding sites per dimeric protein, according to the model shown in Scheme 2. The fitted parameters are summarized in Table 3. We observed that the second putrescine molecule binds with significantly higher affinity to the dimeric protein than the first one. We found that $K_2 > K_1/4$, which implies that putrescine binding to the wild type AdoMetDC protein has positive cooperativity. The cooperativity in a two-site system can be characterized by

$$\Delta\Delta G = -R \cdot T \cdot \ln(4 \cdot K_2 / K_1) \quad (8)$$

We observe that $\Delta\Delta G$ is very significant (Table 3) if we compare it to the ΔG for the total process from the apo to the holo forms. The ΔG for this process is calculated as follows:

$$\Delta G = -R \cdot T \cdot \ln(K_1 \cdot K_2) \quad (9)$$

Figure 4C shows the changes in the population of the different species in equilibrium as a function of the putrescine concentration according to eqs 5, 6 and 7, in Materials and Methods. We observe that the M_2L concentration is never higher than 20% of the total protein, and the high cooperativity favors the binding of the second putrescine molecule (M_2L_2). The stoichiometry of the interaction is consistent with the crystal structure of the human AdoMetDC protein, which shows that each monomer is able to bind one molecule of putrescine (*23, 30, 31*).

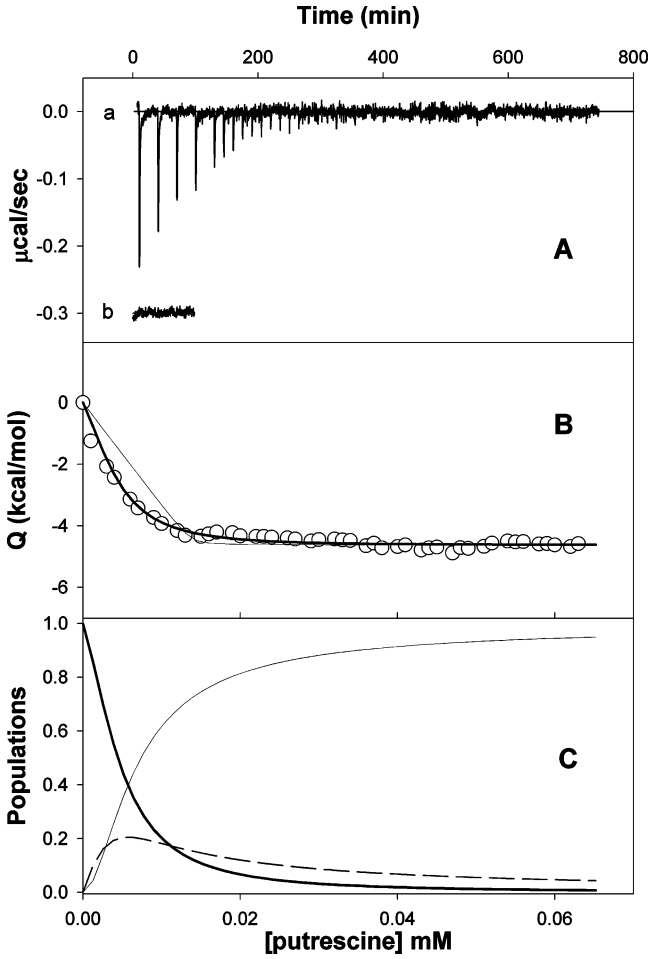

FIGURE 4: Putrescine binding to wild type AdoMetDC by ITC. (A) Representative isothermal titration calorimetry experiment at 15 °C. Heat effects are recorded as a function of time during 45 successive 3 μL injections of 0.70 mM solution of putrescine into the cell containing 0.0138 mM protein (a) or buffer (b). Buffer conditions were 50 mM sodium phosphate at pH 7.5, 1 mM EDTA, and 1 mM TCEP. (B) Cumulative heat effect corresponding to the titration in panel A (o) as a function of putrescine concentration. The thin line is the fit of the experimental data to eq 3. The thick line is the fit of the experimental data to eq 4 with the parameters listed in Table 3. (C) Populations present in solution as a function of putrescine concentration: $[M_2]/[M_T]$ (thick solid line), $[M_2L]/[M_T]$ (dashed line), and $[M_2L_2]/[M_T]$ (thin solid line) calculated according to eqs 5, 6 and 7, respectively.

Table 3: Thermodynamic Parameters for Putrescine Binding to the AdoMetDC Proteins from the ITC Experiments at 15 °C[a]

protein	K_1	K_2	ΔH_1	ΔH_2	ΔG	$\Delta\Delta G$ coop
AdoMetDC(−Put)	9×10^4	3.4×10^5	−5.8	1.2	−13.8[b]	−1.55[c]
E256Q(−Put)	1.0×10^4		−6.1		−10.3[b]	NA
E178Q(−Put)	2.0×10^3		−1.2		−8.7[b]	NA
D174N(−Put)	NE		NE		NE	NA

[a] The binding constants are expressed in M^{-1}, the enthalpies are expressed in kcal per mol of monomer, and free energies are expressed in kcal/mol. The error in the enthalpies and binding constants is ~15%. Note that for E256Q and E178Q, $K_1 = K_2 = K$ and $\Delta H_1 = \Delta H_2$. NA, not applicable; NE, no heat effect was observed for D174N. [b] Calculated according to eq 9. [c] Calculated according to eq 8.

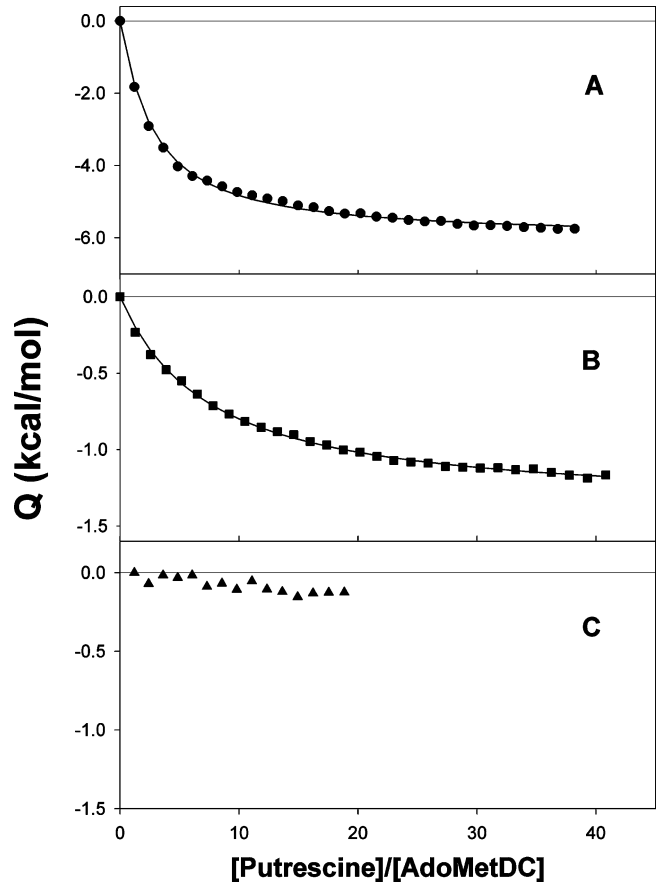

FIGURE 5: Dependence of the heat effect of putrescine binding to AdoMetDC-E256Q (A), AdoMetDC-E178Q (B), and AdoMetDC-D174N (C) as a function of the ratio putrescine/protein. Solid lines are the best fit to eq 3 with the parameters in Table 3.

Figure 5 shows the putrescine binding isotherms for the AdoMetDC mutant proteins at 15 °C. One obvious conclusion can be drawn from these results: the putrescine binding to the D174N variant does not show any significant heat effect (Figure 5C), strongly suggesting that AdoMetDC-D174N is no longer able to bind putrescine. To ensure that the lack of heat effect was due to the lack of binding and not to a very small enthalpy of binding at that temperature or not enough protein concentration, experiments were performed at different temperatures and different protein concentrations (results not shown). In all cases, titration of the D174N variant protein with putrescine produced no significant heat effect under our experimental conditions. Thus, substitution of Asp174 by asparagine abolishes putrescine binding all together.

However, the putrescine binding to the E256Q and E178Q variant proteins shows significant heat effects different from that with wild type AdoMetDC. The isotherms for the E256Q and E178Q can be fitted according to eq 3 (model 1, Figures 5A and B). The fitted parameters are summarized in Table 3. It is obvious from these results that the mechanisms of putrescine interaction with the human AdoMetDC wild type protein and the E256Q, E178Q, and D174N mutant proteins

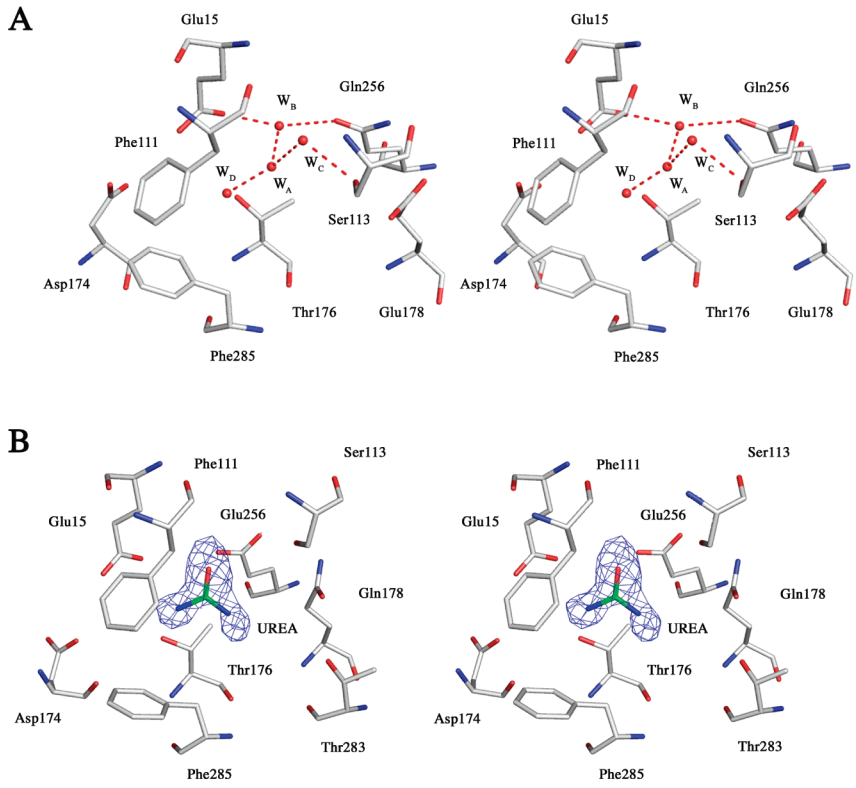

FIGURE 6: Putrescine binding site in the putrescine free mutants. (A) Stereoview of putrescine binding site in the E256Q(−Put) mutant. Water molecules are shown as red spheres, and hydrogen bonds are shown as dashed lines. (B) Stereoview of the putrescine binding site in the E178Q(−Put) mutant. The density maps show a planar ligand comprising four atoms bound in the putrescine binding site. A molecule of urea was modeled into the density. The difference $F_o - F_c$ Fourier map is calculated omitting urea and is contoured at 4.0 σ. The hydrogen bonds are omitted for clarity.

are very different. Substitution of Glu178 or Glu256 by glutamine not only abolishes the positive cooperativity for the binding of the second molecule of putrescine to these proteins but also dramatically decreases the putrescine binding affinity as compared to K_1 for the wild type protein (Table 3).

Crystal Structures of Putrescine Free AdoMetDC. Crystal structures of AdoMetDC(−Put), D174N(−Put), E178Q(−Put), and E256Q(−Put) were obtained. Difference Fourier maps ($F_o - F_c$) and composite omit maps clearly show that putrescine was absent in these structures. Instead, the putrescine binding site in the AdoMetDC(−Put) and D174N(−Put) and E256Q(−Put) mutants contains four additional water molecules (Figure 6A). The nitrogen atom of putrescine closer to the active site is replaced with a water molecule (W_A). This water molecule makes hydrogen bonds to water molecules W_B and W_C, which in turn are hydrogen bonded to Glu256 and Ser113, respectively. A fourth water molecule (W_D) is present roughly at the center of the putrescine binding site and hydrogen bonds to W_A. Asp174 is found in various conformations in the putrescine free structures and is not hydrogen bonded to any conserved water molecule. The structure of the E178Q(−Put) mutant shows a ligand bound in the putrescine binding site. On the basis of the electron density, which is triangular and flat, a molecule of urea was modeled into the putrescine binding site. The carbonyl oxygen of urea occupies the same position as the putrescine amino group closer to the active site and W_A and is hydrogen bonded to the enzyme through water molecules. A stereoview of the ligand bound in the putrescine binding site of the E178Q(−Put) mutant is shown in Figure 6B.

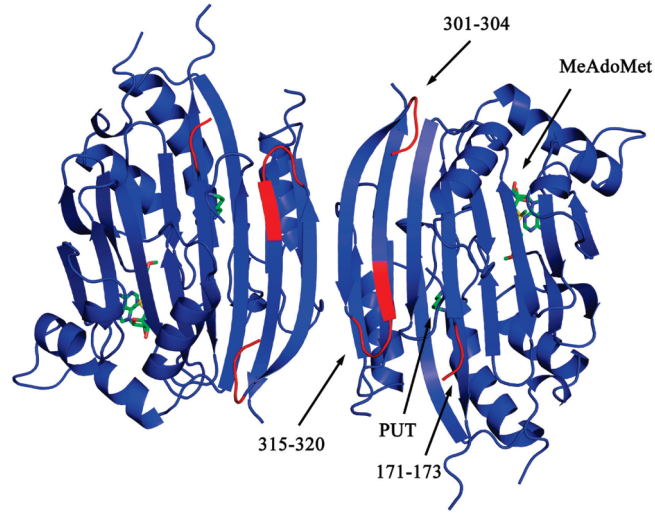

FIGURE 7: Dimeric form of AdoMetDC. Putrescine and MeAdoMet bound in the active site are shown as sticks. There is no overall change in the secondary structure. The loops undergoing conformational change upon putrescine binding are colored red and labeled.

Three regions of the AdoMetDC show differences in the putrescine free structures relative to the putrescine bound structures: residues 171−173, 301−304, and 315−320 (Figure 7). In addition, the side chains of Phe285, Ser 312, and Met314 show different conformation in the putrescine

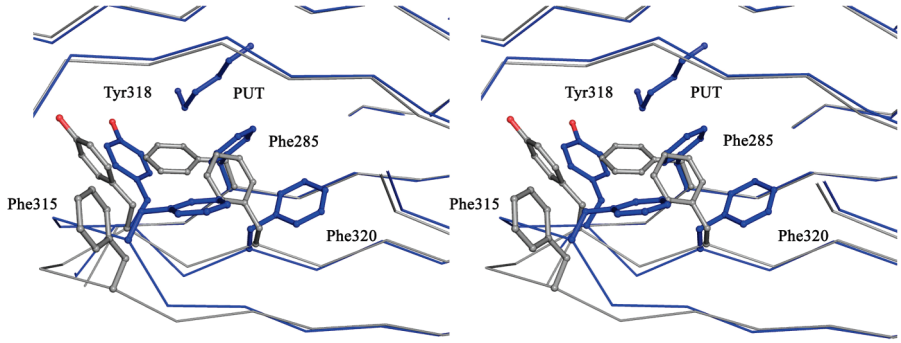

FIGURE 8: Stereoview of the changes in the conformation of aromatic side chains occurring because of putrescine binding. AdoMetDC(+Put) is shown in blue, and AdoMetDC(−Put) is shown in gray. The conformational shift in loop Phe320-Ser312 as an effect of the changes in the aromatic side chains is clearly seen.

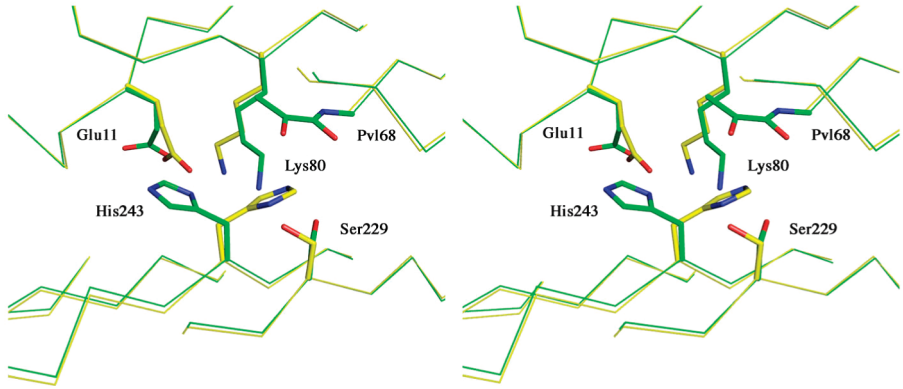

FIGURE 9: Stereoview of the comparison of the catalytic residues His243, Glu11, Lys80, and Ser229 in E256Q(+Put) and E256Q(−Put) mutants. E256Q(+Put) has carbon atoms colored in green, and E256Q(−Put) has carbon atoms colored yellow.

free structures. Loop 171−173 is adjacent to Asp174, which is required for putrescine binding. Four aromatic residues, Phe285, Phe315, Tyr318, and Phe320, are repositioned in the putrescine free structures mostly through changes in the χ_1 torsion angles plus lateral shifts (Figure 8). The repositioning is associated with a 1.5 to 3 Å shift in loop 312−318 and causes the putrescine binding site to become more solvent exposed. The biochemical relevance of loop 301−304 is unclear because it is far away from both the putrescine binding site and the active site.

Crystal Structures of the Putrescine Free AdoMetDC/MeAdoMet Complexes. Complexes of putrescine free mutants with MeAdoMet were prepared to determine the effects of the absence of putrescine on the conformation of the substrate and active site residues. Difference Fourier maps showed MeAdoMet bound in the active site of all three mutants covalently linked to the pyruvoyl cofactor through a Schiff base. The MeAdoMet conformation and the active site are essentially the same as those for the complex of wt-AdoMetDC with MeAdoMet (*30*). The 2′ and 3′ oxygen atoms of the ribose each make a hydrogen bond to the carboxylate group of Glu247. The adenine base stacks between Phe7 and Phe223 with an overall *syn* conformation. All three mutant complexes, including E178Q, showed the same four conserved water molecules in the putrescine binding site. The mutant complexes also showed the same reorganization of the four aromatic residues Phe285, Phe315, Tyr318, and Phe320 and the conformational change in loop 312−320 seen without putrescine and substrate analogue.

Structure of Mutants with Added Putrescine. Structures of E178Q and E256Q were determined after the addition of putrescine. The structure of D174N with putrescine was not determined because biochemical studies reported here show that this mutant does not bind putrescine. For both E178Q(+Put) and E256Q(+Put) addition of putrescine resulted in a reversal of the conformational changes in Phe285, Phe315, Tyr318, and Phe320 and the 312−320 loop seen in the putrescine free structures (Figure 8). The putrescine molecule is in the same position as that observed in all previously reported human AdoMetDC structures (*23, 30, 31*). In both structures, the aliphatic chain of putrescine stacks against Phe111 and Phe285, with the latter residue involved in repositioning the aromatic residues for the putrescine free structures.

In the E256Q(+Put) mutant, one end of putrescine makes direct hydrogen bonds to Glu15, Asp174, and Thr176, while the other end makes water mediated hydrogen bonds to Glu178 and Gln256 as previously observed (*23, 30, 31*). The E178Q(+Put) mutant structure shows some interesting differences. One end of the putrescine molecule makes direct hydrogen bonds to Glu15, Asp174, and Thr176, and the other end of the putrescine makes a water mediated hydrogen bond with Glu256; however, there is no bridging water molecule between putrescine and Gln178. Additionally, compared to all other AdoMetDC structures, there is a conformational change in residues Glu11, Lys80, Ser229, and His243 in E256Q(+Put), which link the putrescine binding site and the active site (Figure 9). The χ_1 torsion angle of His243, which is important for both the processing and decarboxylation reactions, changes from −63° to 90°. In the alternate conformation, the side chain is pointed away from both the pyruvyl cofactor and Ser229. Residues Lys80 and Glu11 also undergo conformational changes and are hydrogen bonded to each other through Ser254 and a water molecule. The other

significant change in E256Q(+Put) is the transformation of the disordered loop 291−299 into a short α-helix. This helix is located at the dimer interface and interacts across the 2-fold axis with the same helix from the other protomer. The closest contact between the two helices is at the sulfur atoms of Cys292, which are 3.6 Å apart.

DISCUSSION

Putrescine Binding to AdoMetDC and Mutants. Activation of the AdoMetDC autoprocessing and decarboxylation reactions is species dependent. The regulation of the polyamine biosynthetic pathway by putrescine in certain species is poorly understood and a thorough understanding of the regulation of polyamine levels might provide an alternate route for inhibiting the pathway. However, the activation of autoprocessing and decarboxylation processes of human AdoMetDC by putrescine and other diamines is well-known and studied (*23*). The rate of activation of the enzyme is highest by putrescine when compared to other diamines. The only previous direct measurements of putrescine binding to AdoMetDC were carried out with the *T. cruzi* enzyme (*29*). The K_d, which was determined by ultrafiltration and by fluorescence change measurements, was 150−180 μM. This is more than an order of magnitude greater than the values measured here by ITC for the human enzyme, but, as described below, it has been shown recently that a much more active enzyme that is not putrescine-activated is formed by a heterodimer between *T. cruzi* AdoMetDC and a structurally homologous regulatory protein (*51*). Although Asp174 appears to be a key residue in binding for both enzymes since mutation to valine in *T. cruzi* (*29*) or asparagine in human (Table 3) abolished binding, it appears that there is little similarity in the activation of the parasite and mammalian enzymes. Our value is much closer to that which would be expected on the basis of the amount of putrescine needed for enzyme activation (K_a of c. 20 μM) (*3, 19*−*21*) or processing (K_a c. 50 μM) (*23*). The latter value may be increased because of competition for binding by nucleic acids in the reticulocyte lysates used for studying processing in coupled transcription/translation systems.

The tight binding of putrescine to human AdoMetDC is also consistent with the difficulty in removing putrescine from the enzyme. This requires extensive dialysis, and it is noteworthy that all of the previously published structures of the protein contain a bound putrescine even though it was not added to the buffers used for crystallization. The current results using ITC confirm that there is only one putrescine binding site in the human AdoMetDC $\alpha\beta$ protomer and rules out postulated models in which two putrescine molecules bring about the changes in AdoMetDC activity (*19, 34, 52*). The previously unrecognized cooperative binding of putrescine to mammalian AdoMetDC is likely to explain the complex kinetics for activation previously reported (*52*). Furthermore, the ITC data confirm that in solution, the putrescine molecule binds in the site identified by the crystal structure. Mutation of Asp174 totally abolished binding, while mutations of Glu178 and Glu256 greatly reduced the affinity for putrescine. Potato AdoMetDC, which is not activated by putrescine, is generally quite similar to the human structure but is an $\alpha\beta$ monomer (*35*). In this structure, several amino acid substitutions in the putrescine binding pocket (Asp174 to valine, Phe111 to arginine, Leu13 to arginine, and Phe285 to histidine) introduce side chains that mimic the role of putrescine in the human enzyme. Thus, dimerization and putrescine activation may be linked.

Structure of the Putrescine Binding Site with and without Putrescine. Previous structural studies clearly identified the putrescine binding site in human AdoMetDC (*23, 30, 31*). Putrescine is bound between the two central β-sheets of the enzyme at a distance of 15 to 20 Å from the active site. The putrescine amino group farther from the active site is directly hydrogen bonded to Asp174, Glu15, and Thr176. The closer amino group is hydrogen bonded through water molecules to Glu178, Glu15, Glu256, and Ser113. The carbon chain of putrescine stacks against Phe285 and Phe111. The crystal structure also shows that there is only one molecule of putrescine bound per monomer.

Previously reported structures provided insights into the mechanism of putrescine activation of human AdoMetDC (*23*). On the basis of these studies, the mechanism of putrescine activation was believed to be due to two reasons. First, putrescine binds inside the β-sandwich region through charge neutralization of acidic residues and hydrophobic interactions to aromatic residues, and it was proposed that stability of the β-sandwich is necessary for the correct orientation of residues for the autoprocessing reaction. Second, there is a hydrogen bonding network from the putrescine binding site to His243, which plays a critical role in the autoprocessing mechanism and in the decarboxylation processes though electrostatics and hydrogen bonding (*23, 33*).

The crystal structures of the putrescine free enzyme and mutants provide newer insights into the putrescine binding site. The putrescine binding site is solvent accessible from one side and in the absence of putrescine the site is filled with water molecules. The comparison of crystal structures of putrescine free and putrescine bound AdoMetDC structures showed no significant changes in the secondary structure. The Far-UV CD experiments have also shown that there is no significant change in the secondary structure of AdoMetDC and the mutants upon putrescine binding, supporting the crystal structures. These observations suggest that putrescine has little effect in stabilizing the secondary structure of the enzyme as previously thought.

Conformational Changes upon Putrescine Binding. Difference distance matrix analysis (*49, 50*) showed significant changes in the Cα positions of residues 171−173, 301−304, and 312−320. Asp174 is required for putrescine binding, and residues 171−173 are near the entrance of the putrescine binding site. Consequently, these residues appear to serve as a gate to the putrescine binding site. In addition, repositioning of the aromatic residues Phe285, Phe315, Tyr318, and Phe320 and the loop containing residues 312−320 further opens the putrescine binding site (Figure 8). Binding of putrescine displaces two water molecules, and Phe285 moves toward the aliphatic portion of the putrescine molecule, followed by closing off of the entrance thus shielding the putrescine from the solvent. These changes result in closer contacts between the protein side chains and an enhancement of electrostatic effects. The near-UV CD experiments showed a small effect for the wt-AdoMetDC and the E256Q mutant, which is due to the change in the aromatic side chain positions. This finding is in agreement

Table 4: Effects of Putrescine on AdoMetDC and Mutants

	putrecine binding[a]	processing[b] (−Put)	processing[c] (+Put)	decarboxylation[d] (−Put)	decarboxylation[e] (+Put)	cooperativity in Put binding[f]
WT	yes	1	5−8	1	4	yes
D174N	no	1	ND	1	ND	ND
E178Q	yes	1	1	4	1	none
E256Q	yes	1	1	1	1	none

[a] As determined by ITC. [b] Relative rate of processing in the absence of putrescine. [c] Relative increase in processing with putrescine added measured at 1 mM Put (*23*). [d] Relative rate of decarboxylation in the absence of putrescine. [e] Relative rate of decarboxylation with putrescine added measured at 0.2 mM Put (*32*). [f] Cooperativity between active sites as determined by ITC.

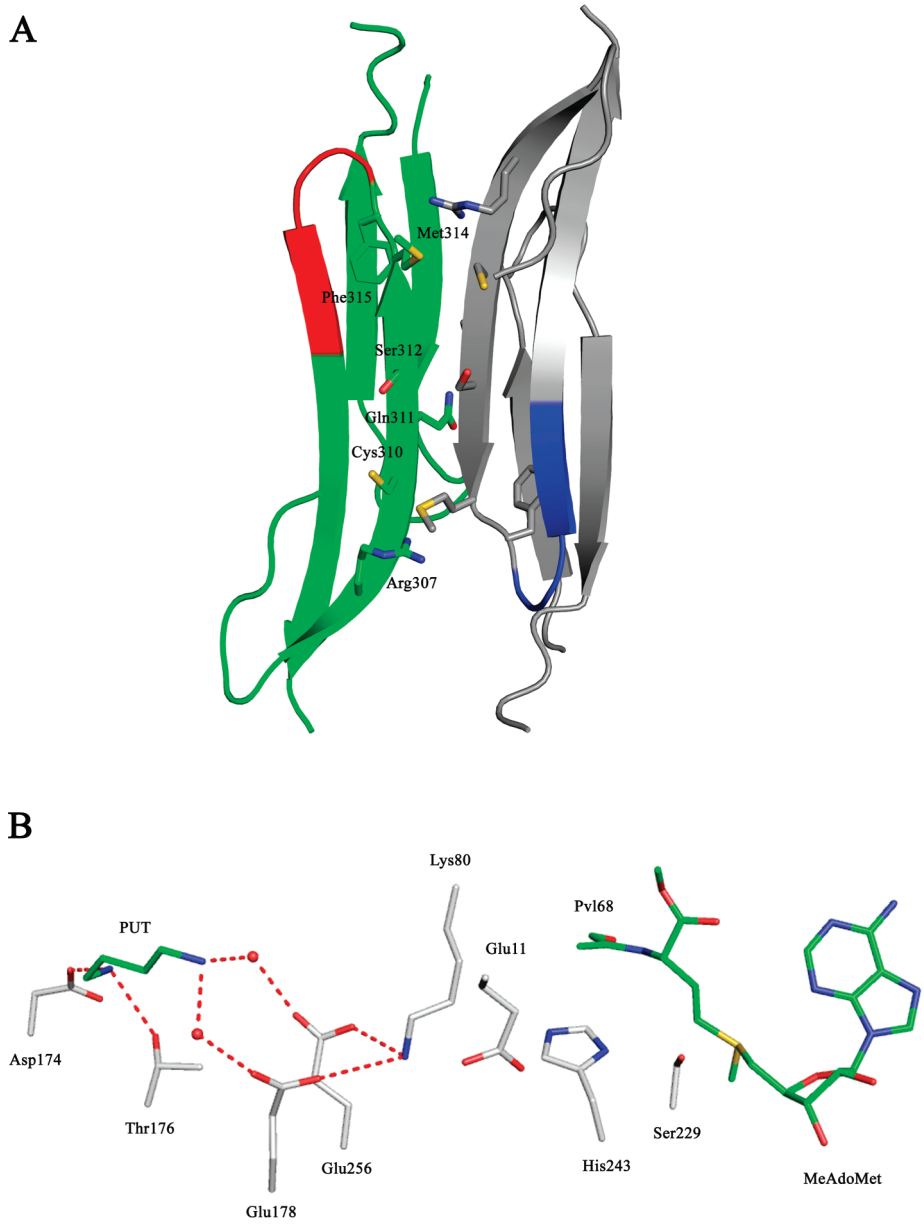

FIGURE 10: (A) Dimer interface of AdoMetDC. The monomers are colored green and gray, respectively. The loop 315−320 is colored red in one monomer and blue in the other. The residues at the interface are shown in sticks. (B) Charge network between the putrescine binding site and the active site. Putrescine, MeAdoMet, and the active site pyruvoyl group carbon atoms are colored green. Water molecules are shown as red spheres, and hydrogen bonds are shown as dashed lines.

with the change in the orientation of Phe285, Phe315, Tyr318, and Phe320 observed upon putrescine binding.

Positive Cooperativity of Putrescine Binding. Human AdoMetDC is a homodimer with two active sites and two putrescine binding sites. ITC studies showed positive cooperativity of putrescine binding for WT-AdoMetDC while no cooperativity was observed for the mutants (Table 4). Loop 312−320, which undergoes a shift upon putrescine binding, is at the dimer interface (Figure 10A). The main contacts between this loop and the 2-fold related protomer occur between the residues Ser312-Ser312′, Met314-Cys310′, Phe315-Arg307′, and Gln311-Gln311′, where the prime designates residues in the 2-fold related protomer. The effect of putrescine binding and conformational changes in the loop

provide a possible mechanism by which changes in one putrescine binding site are relayed through the dimer interface to the putrescine binding site in the other monomer. Not consistent with this argument is that the E178Q and E256Q mutants bind putrescine but do not show cooperativity even though the same conformational changes are observed upon putrescine binding for loop 312−320 and the four aromatic residues, suggesting that other factors are involved.

Structural Insights into Putrescine Stimulation of AdoMetDC Activity. Structural comparisons suggest no global conformational changes upon putrescine binding to AdoMetDC; however, several local conformational changes are observed. This suggests that the primary effect of putrescine is electrostatic and that this effect is transmitted to the active site though hydrogen bonding (Figure 10B). Binding of putrescine introduces two positive charges into a binding pocket that contains three conserved acidic residues. Glu178 and Glu256 are hydrogen bonded through water to the putrescine amino group closer to the active site and are near Lys80, which is disordered in most AdoMetDC structures. Lys80 is also near Glu11 and His243, two residues important for both autoprocessing and catalysis. Through this network, the pK_a of His243 would increase in the presence of putrescine and decrease in its absence. The side chain of Glu11 is positioned to assist in protonation/deprotonation of the His243. Glu11 is an essential residue for the activation by putrescine, although it plays no direct role in putrescine binding. Mutation of Glu11 to glutamine abolishes putrescine activation of processing (*34*), and mutation to aspartate causes putrescine to be an inhibitor of processing (*23*). Mutation E11K prevents processing completely (*34*). Mutation E11Q greatly reduces AdoMetDC activity (*34*) and reduces the stimulation by putrescine by 60%. The E11D change reduces activity of the processed enzyme by about 4-fold and putrescine activation by about 50% (unpublished work). The mutant K80A has only about 10% activity and is stimulated by putrescine only at very high concentrations with a K_a of 400 μM. Similarly, the processing of this mutant is much slower than wild type and is putrescine activated but requires much higher levels of putrescine (K_a of c. 1 mM). Combination of the K80A/E11D mutation abolishes the inhibitory effect on processing of this mutation and the K80A and K80A/E11D mutants have identical responses to putrescine (unpublished work).

ITC binding results show that the D174N mutant protein does not bind putrescine. The E178Q and E256Q mutants bind putrescine but show no stimulation of processing. The negative charge appears to be key for influencing active site electrostatics, and its absence blocks the effects of putrescine. In contrast, the E178Q mutant has decarboxylation activity in the absence of putrescine comparable to wild type with putrescine, while the decarboxylation activity of the E256Q mutant is not simulated by putrescine. These results are consistent with a proposed model of charge relay through Lys80 to Glu11 to His243 resulting from putrescine binding.

Another possibility is that putrescine utilizes electrostatic interactions to correctly position active site residues. Evidence for a structural switch comes from the structure of the E256Q(+Put), which shows conformational changes in Glu11, Lys80, Ser229, and His243. The largest change occurs in His243, which rotates about its χ_1 torsion angle by about 150°. In this conformation, the side chain is pointed away from both the pyruvoyl cofactor and Ser229. Previous biochemical data show that the catalytic activity of the E256Q(−Put) mutant is far lower than the wild type enzyme and is not stimulated by the addition of putrescine (*32*), suggesting this positioning of residues represents a low activity state in which putrescine is unable to influence the correct positioning of active site residues. The structure E178Q(+Put) lacks a bridging water molecule between putrescine and Gln178, resulting in no activation of the E178Q(−Put) mutant by putrescine.

Implications for Other AdoMetDCs. The effect of putrescine varies among species. Class 1a and 1b enzymes have a fold that is similar to both the N-terminal and C-terminal halves of the class 2 protomer; however, class 1 AdoMetDCs do not have a putrescine binding site and are not stimulated by putrescine. Class 2a AdoMetDCs include the plant enzymes and have a fold very similar to that of the class 1a protomer but are monomeric rather than dimeric (*35*). The class 2a enzymes contain a buried cluster of charged residues that is reminiscent of the putrescine binding site found in human AdoMetDC; however, the pocket is filled by two arginine residues that are not present in any class 2b enzyme. Class 2a AdoMetDCs are not stimulated by putrescine but have constitutive processing and decarboxylation activities similar to those of the putrescine activated human AdoMetDC.

Multiple sequence alignments show that all of the key active site residues are conserved in the class 2a and class 2b AdoMetDCs as are the residues that connect the buried charged cluster. Class 2a and 2b are distinguished in part by the nature of the buried cluster. Within class 2b, there are two subclasses. The first is represented by human AdoMetDC and is distinguished by a conserved Lys80. Within this group, the three acidic residues in the putrescine binding site are conserved. The four aromatic residues are not entirely conserved; however, these residues are always aromatic or large hydrophobic residues. The second subclass includes apicomplexan parasites and is distinguished by the substitution of isoleucine in place of Lys80. A hydrophobic residue would interrupt the electrostatic transfer of charge and suggests that putrescine stimulates this group of AdoMetDCs by a different mechanism than that of human AdoMetDC. Studies on the *Trypanosome brucei* AdoMetDC showed that putrescine stimulates the decarboxylation reaction; however, the activity was about 1000-fold lower than the activity of the human AdoMetDC (*51*). Recently, Phillips and co-workers showed that formation of a heterodimer between AdoMetDC and a structurally homologous but inactive regulatory protein resulted in decarboxylation rates comparable to that of human AdoMetDC (*51*). Furthermore, the heterodimeric *T. brucei* AdoMetDC was not stimulated by the addition of putrescine. No structures are available for this group of AdoMetDCs, and the mechanism of stimulation remains to be determined.

Regulating polyamine levels by controlling the enzymes in the polyamine biosynthetic pathway is a promising target for cancer and antiparasitic therapy (*6, 7*). Our results suggest that an alternate approach to inhibiting AdoMetDC would be to target the putrescine binding site. Compounds binding to this site that mimic the effects of some of the mutants described above may prevent processing or significantly block activity.

ACKNOWLEDGMENT

We thank Leslie Kinsland for assistance in the preparation of the manuscript. We thank NE-CAT of the Advanced Photon Source and CHESS for providing beam time and assistance with data collection.

REFERENCES

1. Tabor, C. W., and Tabor, H. (1984) Methionine adenosyltransferase (*S*-adenosylmethionine synthetase) and *S*-adenosylmethionine decarboxylase. *Adv. Enzymol. Relat. Areas Mol. Biol. 56*, 251–282.
2. Pegg, A. E. (1986) Recent advances in the biochemistry of polyamines in eukaryotes. *Biochem. J. 234*, 249–262.
3. Pegg, A. E., Xiong, H., Feith, D., and Shantz, L. M. (1998) *S*-adenosylmethionine decarboxylase: structure, function and regulation by polyamines. *Biochem. Soc. Trans. 26*, 580–586.
4. Li, Y. F., Hess, S., Pannell, L. K., Tabor, C. W., and Tabor, H. (2001) In vivo mechanism-based inactivation of *S*-adenosylmethionine decarboxylases from *Escherichia coli*, *Salmonella thyphimurium*, and *Saccharomyces cerevisiae*. *Proc. Natl. Acad. Sci. U.S.A. 98*, 10578–10583.
5. Hackert, M. L., and Pegg, A. E. (1997) Pyruvoyl-Dependent Enzymes, in *Comprehensive Biological Catalysis* (Sinnott, M. L., Ed.), pp 201−216, Academic Press, London.
6. van Poelje, P. D., and Snell, E. E. (1990) Pyruvoyl-dependent enzymes. *Annu. Rev. Biochem. 59*, 29–59.
7. Wallace, H. M., Fraser, A. V., and Hughes, A. (2003) A perspective of polyamine metabolism. *Biochem. J. 376*, 1–14.
8. Mihich, E. (1963) Current Studies with Methylglyoxal-Bis(Guanylhydrazone). *Cancer Res. 23*, 1375–1389.
9. Regenass, U., Mett, H., Stanek, J., Mueller, M., Kramer, D., and Porter, C. W. (1994) CGP 48664, a new *S*-adenosylmethionine decarboxylase inhibitor with broad spectrum antiproliferative and antitumor activity. *Cancer Res. 54*, 3210–3217.
10. Eskens, F. A., Greim, G. A., van Zuylen, C., Wolff, I., Denis, L. J., Planting, A. S., Muskiet, F. A., Wanders, J., Barbet, N. C., Choi, L., Capdeville, R., Verweij, J., Hanauske, A. R., and Bruntsch, U. (2000) Phase I and pharmacological study of the weekly administration of the polyamine synthesis inhibitor SAM 486A (CGP 48 664) in patients with solid tumors. European Organization for Research and Treatment of Cancer Early Clinical Studies Group. *Clin. Cancer Res. 6*, 1736–1743.
11. Zhou, H., Choi, L., Lau, H., Bruntsch, U., Vries, E. E., Eckhardt, G., Oosterom, A. T., Verweij, J., Schran, H., Barbet, N., Linnartz, R., and Capdeville, R. (2000) Population pharmacokinetics/toxicodynamics (PK/TD) relationships of SAM486A in phase I studies in patients with advanced cancers. *J. Clin. Pharmacol. 40*, 275–283.
12. Paridaens, R., Uges, D. R. A., Barbet, N., Choi, L., Seeghers, M., van der Graaf, W. T. A., and Groen, J. J. M. (2000) A phase I study of a new polyamine biosynthesis inhibitor, SAM486A, in cancer patients with solid tumours. *Br. J. Cancer 83*, 594–601.
13. Siu, L. L., Rowinsky, E. K., Hammond, L. A., Weiss, G. R., Hidalgo, M., Clark, G. M., Moczygemba, J., Choi, L., Linnartz, R., Barbet, N. C., Sklenar, I. T., Capdeville, R., Gan, G., Porter, C. W., Von Hoff, D. D., and Eckhardt, S. G. (2002) A phase I and pharmacokinetic study of SAM486A, a novel polyamine biosynthesis inhibitor, administered on a daily-times-five every-three-week schedule in patients with Advanced solid malignancies. *Clin. Cancer. Res. 8*, 2157–2166.
14. van Zuylen, L., Eskens, F., Bridgewater, J., Sparreboom, A., Sklenar, I., Planting, A., Choi, L., Mueller, C., Capdeville, R., Ledermann, J., and Verweij, J. (2000) The Polyamine synthesis inhibitor SAM486A in combination, with 5-FU/LV in metastatic colorectal cancer (MCC): Results of a phase I and pharmacokinetic study. *Proc. Am. Soc. Clin. Oncol. 36*, 751.
15. Pless, M., Belhadj, K., Kern, W., Dumontet, C., Chemnitz, J., Menssen, H. D., Herrmann, R., Barbet, N. C., and Capdeville, R. (2000) Clinical efficacy of SAM486A, a novel polyamine biosynthesis inhibitor, in patients with refractory or relapsed non-Hodgkin's lymphoma. *Proc. Am. Soc. Clin. Oncol. 36*, 62.
16. Millward, M. J., Joshua, A., Kefford, R., Aamdal, S., Thomson, D., Hersey, P., Toner, G., and Lynch, K. (2005) Multi-centre Phase II trial of the polyamine synthesis inhibitor SAM486A (CGP48664) in patients with metastatic melanoma. *Invest. New Drugs 23*, 253–256.
17. Toms, A. V., Kinsland, C., McCloskey, D. E., Pegg, A. E., and Ealick, S. E. (2004) Evolutionary links as revealed by the structure of *Thermotoga maritima* S-adenosylmethionine decarboxylase. *J. Biol. Chem. 279*, 33837–33846.
18. Ekstrom, J. E., Matthews, I. I., Stanley, B. A., Pegg, A. E., and Ealick, S. E. (1999) The crystal structure of human *S*-adenosylmethionine decarboxylase at 2.25 Å resolution reveals a novel fold. *Structure 7*, 583–595.
19. Stanley, B. A. (1995) Mammalian *S*-Adenosylmethionine Decarboxylase Regulation and Processing, in *Polyamines: Regulation and Molecular Interaction* (Casero, R. A., Ed.) pp 27−75, R. G. Landes Co., Austin, TX.
20. Pegg, A. E. (1984) S-adenosylmethionine decarboxylase: a brief review. *Cell Biochem. Function 2*, 11–15.
21. Pegg, A. E., and Williams-Ashman, H. G. (1969) On the role of *S*-adenosyl-L-methionine in the biosynthesis of spermidine by the rat prostate. *J. Biol. Chem. 244*, 682–693.
22. Beswick, T. C., Willert, E. K., and Phillips, M. A. (2006) Mechanisms of allosteric regulation of *Trypanosoma cruzi S*-adenosylmethionine decarboxylase. *Biochemistry 45*, 7797–7807.
23. Ekstrom, J. L., Tolbert, W. D., Xiong, H., Pegg, A. E., and Ealick, S. E. (2001) Structure of a human *S*-adenosylmethionine decarboxylase self-processing ester intermediate and mechanism of putrescine stimulation of processing as revealed by the H243A mutant. *Biochemistry 40*, 9495–9504.
24. Mamont, P. S., Danzin, C., Wagner, J., Siat, M., Joder-Ohlenbusch, A., and Claverie, N. (1982) Accumulation of decarboxylated *S*-adenosylmethionine in mammalian cells as a consequence of the inhibition of putrescine synthesis. *Eur. J. Biochem. 123*, 499–504.
25. Hibasami, H., Hoffman, J. L., and Pegg, A. E. (1980) Decarboxylated S-adenosylmethionine in mammalian cells. *J. Biol. Chem. 255*, 6675–6678.
26. Tekwani, B. L., Bacchi, C. J., and Pegg, A. E. (1992) Putrescine activated S-adenosylmethionine decarboxylase from *Trypanosoma brucei brucei*. *Mol. Biochem. Biochem. 117*, 53–61.
27. Persson, K., Aslund, L., Grahn, B., Hanke, J., and Heby, O. (1998) *Trypanosoma cruzi* has not lost its *S*-adenosylmethionine decarboxylase: characterization of the gene and the encoded enzyme. *Biochem. J. 333*, 527–537.
28. Hoyt, M. A., Williams-Abbott, L. J., Pitkin, J. W., and Davis, R. H. (2000) Cloning and expression of the *S*-adenosylmethionine decarboxylase gene of *Neurospora crassa* and processing of its product. *Mol. Gen. Genet. 263*, 664–673.
29. Clyne, T., Kinch, L. N., and Phillips, M. A. (2002) Putrescine activation of *Trypanosoma cruzi S*-adenosylmethionine decarboxylase. *Biochemistry 41*, 13207–13216.
30. Tolbert, D. W., Ekstrom, J. L., Mathews, I. I., Secrist, J. A. I., Kapoor, P., Pegg, A. E., and Ealick, S. E. (2001) The structural basis for substrate specificity and inhibition of human *S*-adenosylmethionine decarboxylase. *Biochemistry 40*, 9484–9494.
31. Tolbert, W. D., Zhang, Y., Cottet, S. E., Bennett, E. M., Ekstrom, J. L., Pegg, A. E., and Ealick, S. E. (2003) Mechanism of human *S*-adenosylmethionine decarboxylase proenzyme processing as revealed by the structure of the S68A mutant. *Biochemistry 42*, 2386–2395.
32. Stanley, B. A., Shantz, L. M., and Pegg, A. E. (1994) Expression of mammalian *S*-adenosylmethionine decarboxylase in *Escherichia coli*. Determination of sites for putrescine activation of activity and processing. *J. Biol. Chem. 269*, 7901–7907.
33. Xiong, H., Stanley, B. A., Tekwani, B. L., and Pegg, A. E. (1997) Processing of mammalian and plant *S*-adenosylmethionine decarboxylase proenzymes. *J. Biol. Chem. 272*, 28342–28348.
34. Stanley, B. A., and Pegg, A. E. (1991) Amino acid residues necessary for putrescine stimulation of human *S*-adenosylmethionine decarboxylase proenzyme processing and catalytic activity. *J. Biol. Chem. 266*, 18502–18506.
35. Bennett, E. M., Ekstrom, J. L., Pegg, A. E., and Ealick, S. E. (2002) Monomeric *S*-adenosylmethionine decarboxylase from plants provides an alternative to putrescine stimulation. *Biochemistry 41*, 14509–14517.
36. Liu, L., Xu-Welliver, M., Kanugula, S., and Pegg, A. E. (2002) Inactivation and degradation of O(6)-alkylguanine-DNA alkyltransferase after reaction with nitric oxide. *Cancer Res. 62*, 3037–3043.
37. Winder, A. F., and Gent, W. L. (1971) Correction of light-scattering errors in spectrophotometric protein determinations. *Biopolymers 10*, 1243–1251.
38. Makhatadze, G. I., Medvedkin, V. N., and Privalov, P. L. (1990) Partial molar volumes of polypeptides and their constituent groups

in aqueous solution over a broad temperature range. *Biopolymers 30*, 1001–1010.
39. Lopez, M. M., and Makhatadze, G. I. (2002) Isothermal titration calorimetry. *Methods Mol. Biol. 173*, 121–126.
40. Brokx, R. D., Lopez, M. M., Vogel, H. J., and Makhatadze, G. I. (2001) Energetics of target peptide binding by calmodulin reveals different modes of binding. *J. Biol. Chem. 276*, 14083–14091.
41. Indyk, L., and Fisher, H. F. (1998) Theoretical aspects of isothermal titration calorimetry. *Methods Enzymol. 295*, 350–364.
42. Lopez, M. M., Yutani, K., and Makhatadze, G. I. (1999) Interactions of the major cold shock protein of *Bacillus subtilis* CspB with single-stranded DNA templates of different base composition. *J. Biol. Chem. 274*, 33601–33608.
43. Seiler, N., and Knödgen, B. (1980) High performance liquid chromatographic procedure for the simultaneous determination of the natural polyamines and their monoacetyl derivatives. *J. Chromatogr. 221*, 227–235.
44. Otwinowski, Z., and Minor, W. (1997) Processing of x-ray diffraction data collected in oscillation mode. *Methods Enzymol. 276*, 307–326.
45. Brünger, A. T., Adams, P. D., Clore, G. M., DeLano, W. L., Gros, P., Grosse-Kunstleve, R. W., Jiang, J. S., Kuszewski, J., Nilges, M., Pannu, N. S., Read, R. J., Rice, L. M., Simonson, T., and Warren, G. L. (1998) Crystallography & NMR system: A new software suite for macromolecular structure determination. *Acta Crystallogr., Sect. D 54*, 905–921.
46. Jones, T. A., Zou, J.-Y., Cowan, S. W., and Kjeldgaard, M. (1991) Improved methods for the building of protein models in electron density maps and the location of errors in these models. *Acta Crystallogr., Sect. A 47*, 110–119.
47. Emsley, P., and Cowtan, K. (2004) Coot: model-building tools for molecular graphics. *Acta Crystallogr., Sect. D 60*, 2126–2132.
48. Kleywegt, G. J., and Jones, T. A. (1998) Databases in protein crystallography. *Acta Crystallogr., Sect. D 54*, 1119–1131.
49. Richards, F. M., and Kundrot, C. E. (1988) Identification of structural motifs from protein coordinate data: secondary structure and first-level supersecondary structure. *Proteins 3*, 71–84.
50. Schneider, T. R. (2004) Domain identification by iterative analysis of error-scaled difference distance matrices. *Acta Crystallogr., Sect. D 60*, 2269–2275.
51. Willert, E. K., Fitzpatrick, R., and Phillips, M. A. (2007) Allosteric regulation of an essential trypanosome polyamine biosynthetic enzyme by a catalytically dead homolog. *Proc. Natl. Acad. Sci. U.S.A. 104*, 8275–8280.
52. Dezeure, F., Gerhart, F., and Seiler, N. (1989) Activation of rat liver *S*-adenosylmethionine decarboxylase by putrescine and 2-substituted 1,4 butanediamines. *Int. J. Biochem. 21*, 889–899.

BI801732M